# A CONCENTRIC ELLIPSE MULTIPLE-ARCH SYSTEM IN THE SOLAR CORONA

KUNIJI SAITO*

*Tokyo Astronomical Observatory and Sacramento Peak Observatory, Air Force Cambridge Research Laboratories, Sunspot, N.M., U.S.A.*

and

CHARLES L. HYDER

*Sacramento Peak Observatory, Air Force Cambridge Research Laboratories, Sunspot, N.M., U.S.A.*

(Received 13 March, 1968)

**Abstract.** A typical concentric ellipse multiple-arch system was observed in the solar corona during the February 4, 1962 eclipse in New Guinea. The following results have been obtained from analysis of a white-light photograph taken by N. Owaki (see OWAKI and SAITO, 1967a).

(1) The arches are composed of four equidistant components, elliptical in shape, and almost concentric with a prominence at the common center of the ellipses.

(2) The prominence and arch system appears to be the lower region of a helmet-shaped streamer.

(3) The widths of the arches are observed to increase with height.

(4) Analysis was made in the light of three models for the coronal structures that could lead to the observed arches: (a) rod-like concentrations of electrons; (b) tunnel-shaped elliptical shells of electrons; and (c) dome-like ellipsoidal shells of electrons. Electron densities are derived for the models, and the dome-like model is excluded as a possibility for arch systems exhibiting a coronal cavity.

(5) The scale height in the arch-streamer region is found to be almost the same as that of the K-corona, suggesting equal temperatures, density distributions, etc. in each region.

(6) There is a dark space (a coronal cavity) between the innermost arch and the prominence. The brightness of this cavity is $\frac{1}{3}$ that of the adjacent arch. It is 3% brighter than the background corona of the arch-streamer system.

(7) A comparison is made between the deficiency of electrons in the coronal cavity and the excess of electrons in the prominence. It is found that the ratio of the excess to the deficiency lies between 0.9 and 40.

(8) A comparison between the electron efflux from the 'leaky magnetic bottle' possibly formed by rod-shaped coronal arches and the electron influx into those arches from the chromosphere leads us to the conclusion that the rod model is probably valid and that spicules appear to be an adequate supply for the electrons observed in the arches. The tunnel model may be valid, but in that case spicules are probably not the sources of the electrons observed in coronal arches.

## 1. Introduction

The multiple-arch systems surrounding quiescent prominences have long drawn the attention of eclipse observers. BALANOVSKY and PEREPELKIN (1928) noticed two arch systems over prominences when they photographed the brightness distribution in the white-light corona during the June 29, 1927 eclipse in North Sweden. They give a map of detailed isophotic curves for two bright and two dark nearly concentric arches at P.A. 140°.

* Member of the High Altitude Observatory Solar Project supported under contract F 19628-67-C-0231.

VON KLÜBER (1961) made a photometric study of the inner corona at the above eclipse. He measured the coronal plates obtained by the Hamburg-Bergedorf Observatory expedition sent to Lapland. He studied one of the arches described by Balanovsky and Perepelkin at P.A. 143°. He is inclined to think of the observed formation as concentric domes seen in projection rather than rod-like arches. We shall discuss this point in detail in Section 5.

WALLENQUIST (1957) noticed a multiple-arch system at P.A. 114° on the coronal plate taken during the June 30, 1954 eclipse in Gotland, Sweden.

LEROY and SERVAJEAN (1966) took a color photograph of the corona during the May 30, 1965 eclipse in the South Pacific (LEROY, 1966). They found a multiple-arch system over a prominence at P.A. 38°. They measured a brightness decrease of about 7% in a low-intensity zone between the innermost arch and prominence.

Recently KAWAGUCHI (1967) has conducted a detailed photometric investigation of an arch formation observed by Bigay at P.A. 142° during the February 15, 1961 eclipse. Kawaguchi interpreted the bright arch as an aggregate of free electrons trapped in a gigantic rod-like bundle of magnetic lines of force and calculated the electron density along the arch and found the degree of concentration in the cross-section to be least at the top of the arch and increasing with decreasing height. He also noticed a dark space, or coronal cavity, over the prominence.

Detailed geometric, polarimetric and photometric investigations of arch systems will give information about physical relations between the corona and the associated prominences. Unfortunately, the faintness and small dimensions of the features have so far prevented us from deriving data of satisfactory precision. As Leroy and Servajean state, the necessary conditions in order to obtain any photographs suitable for present purposes will be: (1) satisfactory optical resolution; practically, a longer focal length camera, say, a few meters; and (2) satisfactory exposure time for photographing the whole feature.

Most of the observations mentioned above are large-scale photographs, so they satisfy the first condition, but some of them are far from fulfilling the second condition. For example, the Bigay photograph which Kawaguchi investigated shows only one bright and dark arch over a prominence. It is probable, however, that if a longer exposure had been used, a few outer arches would have appeared concentric with the lower arch. On the other hand, a longer exposure would have given rise to a terrible over-exposure in the inner arches. So, a third advisable condition for photographing these faint objects is: (3) use of a device which will neutralize the steep brightness decrement of the inner corona and show the whole extent of the arch system above the background corona.

In practice, a rotating sector vane placed at the focus of the camera has been used, e.g., by LAFFINEUR *et al.* (1961), SMITH *et al.* (1965), OWAKI and SAITO (1967), and SAITO and OWAKI (1967) to see more of the corona on a single exposure. During the November 12, 1966 eclipse a radially graded neutral density filter was first employed successfully by NEWKIRK (1967; see also MALVILLE, 1967). This new method seems to be superior to the sector method since the former is free from the photographic

intermittency effects, and it can be made to give a more uniform picture than has been possible with rotating sectors.

In the present study we consider a typical multiple-arch system overlying a prominence at P.A. 240° in the coronal photograph which was taken by N. Owaki at the February 4, 1962 eclipse in New Guinea. We also try to build a model of the arch system by using the present and older data. The present photograph satisfactorily fulfills the three conditions of white-light coronal photography as the following data indicate: (1) the horizontal eclipse camera used by Owaki yields a solar image about 5 cm in diameter; (2) the exposure time was 20 sec; and (3) a rotating sector vane driven at a speed of 750 r.p.m. was used to enhance the fainter outer area.

An enlarged reproduction of the multiple-arch system is given in Figure 1. It represents four bright, almost concentric arches and a helmet-shaped streamer that enveloped the arch system. The dark shadow to the right part of the photograph was produced by the supports of the rotating sector and a driving motor. Circular bright and dark bands concentric with the sun were made by the unsuitable shape of the sector vane.

## 2. Microdensitometry and Calibrations

Microdensitometry of the Owaki photograph was carried out over a fan-shaped area of the corona centered on the arch system from P.A. 210° to 260°. The microdensitometer aperture was a 0.03 mm square projected on the film. The diameter of the sun was 47.34 mm. A total of 36 concentric traces was obtained in the range $0.05 \leq r \leq 3.59\ R_\odot$ at variable intervals from $\Delta r = 0.02\ R_\odot$ in the innermost part of the corona to $\Delta r = 0.46\ R_\odot$ in the outermost part. Radial traces were also made every one degree. Both sets of tracings were referenced to the sector center.

The following calibrations were made:

(1) The sector vane had been designed to compensate for the brightness distribution of the Van de Hulst model corona ($K_{min.equ.} + F$). Calibration was applied by measuring the angles of sector openings at respective radii. Corrections for the sector shape cancelled the observed circular stripes seen in Figure 1.

(2) The photographic intermittency effect was thoroughly investigated in the laboratory by varying the sector openings and illuminations on the focus. Details of this investigation are given elsewhere (OWAKI and SAITO, 1967). A correction of brightness for this effect of 0.05 in the logarithm was required on the average while the maximum correction was 0.14 in the logarithm in a few extreme cases.

(3) The present exposure of the corona was taken near mid-totality, so the displacement between the centers of the sun and moon was $0.004\ R_\odot$. But the difference between the centers of the sun and sector was found to be $0.024\ R_\odot$. The coordinate origin was adjusted to the sun's center.

(4) The present photometry was only given in relative values of brightness. In order to express them in absolute units, the results were compared with the SAITO and HATA (1964) data over a large common area of the corona. The method of absolute photometry which Saito and Hata used at this eclipse is to measure the direct illumi-

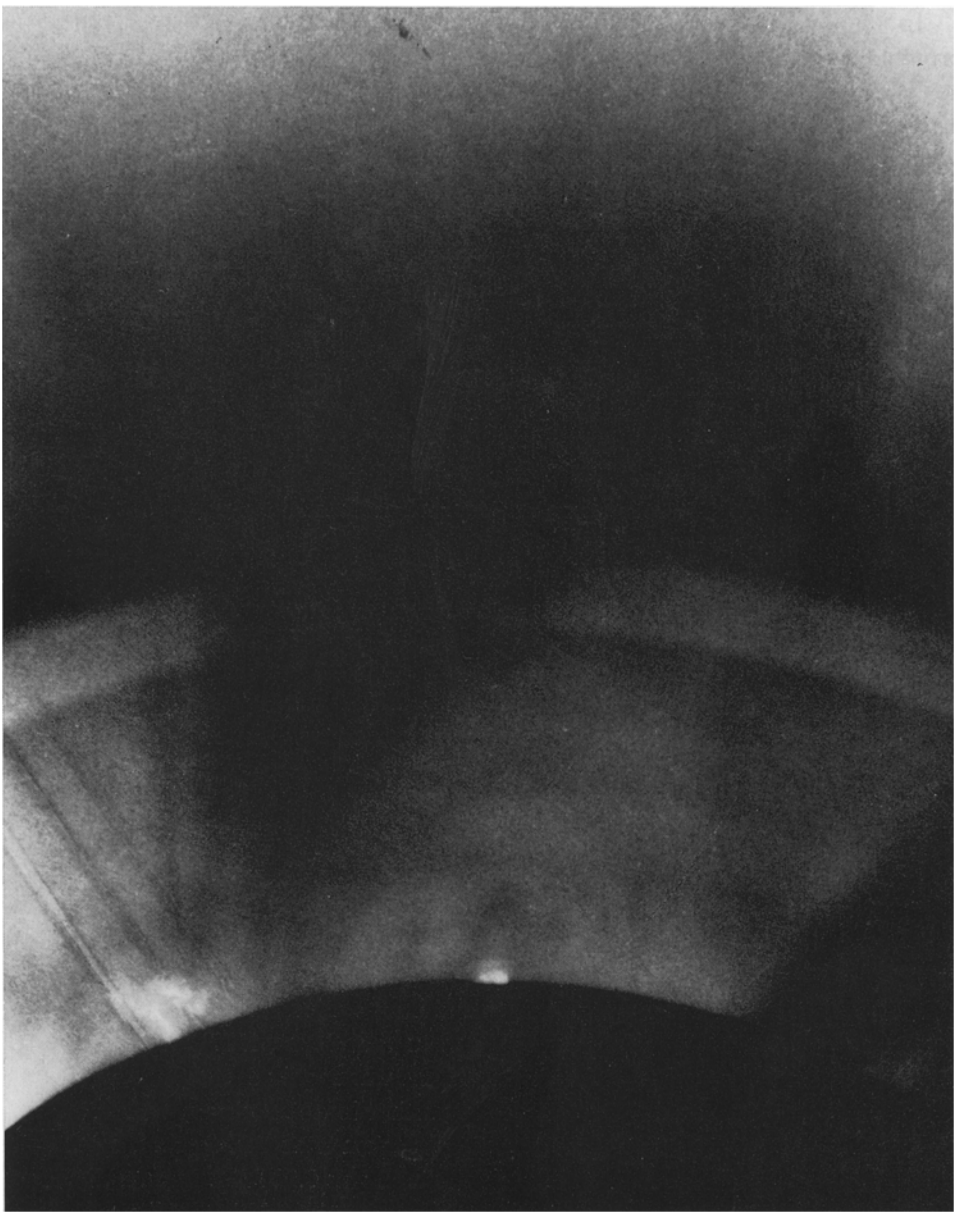

Fig. 1. The multiple-arch system appeared over a prominence at P.A. 240° on the eclipse plate taken by N. Owaki at the February 4, 1962 eclipse in New Guinea. A camera of 5-m focal length provided with a rotating sector was used.

nation of the solar disk photographically by diluting the sun's intensity by known factors with a set of light-diffusing tubes.

In Figure 2 we show the brightness distribution of the observed white-light corona from P.A. 210° to P.A. 260°. The ordinates are the logarithm of the ratio of the observed brightness to the average solar brightness ($\bar{B}_\odot$), and the abscissae are the heliographic position angles. A total of 36 curves correspond to the brightness at solar distances assigned to respective curves expressed in $R_\odot$. Superposed on the brightness curves are the patterns of the prominence, arches and accompanying rays. These patterns are not correctly expressed topologically since the figure does not give the isophotic curves.

Note that the figure shows a low-intensity valley through the curves starting at P.A. 253° at the sun's limb, and extending beyond $r/R_\odot = 3.59$. This less intense, or quiet, region of the corona will be designated as $B^*$. If the brightness values from this quiet portion are subtracted from the corresponding values of the arch-streamer

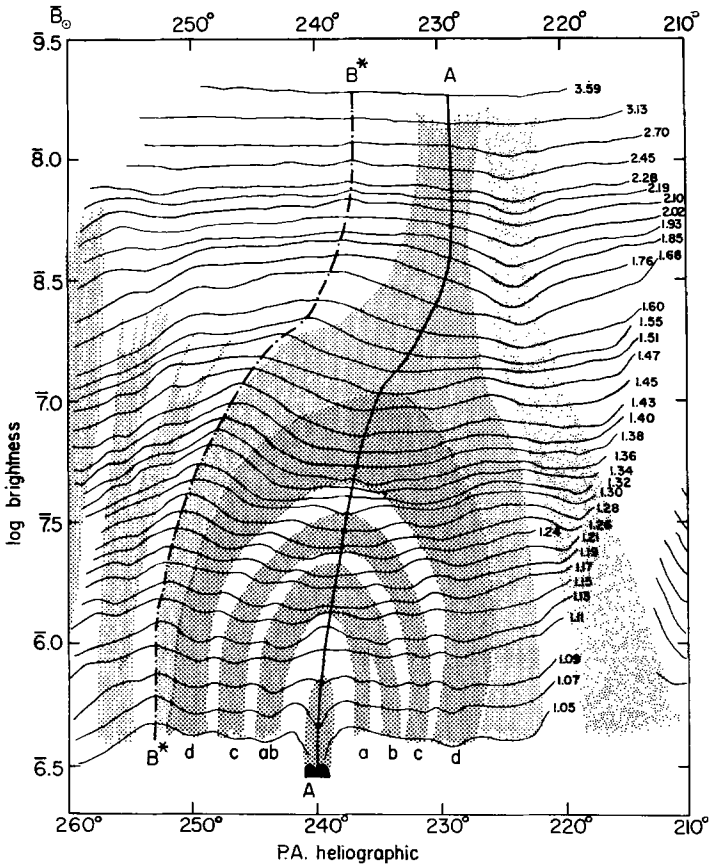


Fig. 2. Microphotometric traces of the multiple-arch system and its neighborhood on the February 4, 1962 eclipse photograph. The arches are found composed of four components. $A$ and $B^*$ represent the axes of the system and the background corona, respectively.

region, the contribution of present interest $(B-B^*)_{abs}$ remains. Thus, the general corona and F-corona as well as the sky brightness and scattered light during totality are automatically eliminated. In spite of some possible ambiguity in selecting the $B^*$ values, a satisfactory conclusion was obtained since the values $(B-B^*)_{abs}$ do not become negative anywhere in the observed region and become very small far from the area of activity. The axis of the arch system, designated as $A$ in Figure 2, initiates at P.A. 240°, and tends to the South higher up.

## 3. Geometric Results

In Figure 3 we show a drawing of the arch system with a coordinate network and indications of the limbs of the sun and moon, the locus of $B^*$ and the axis of the system $A$.

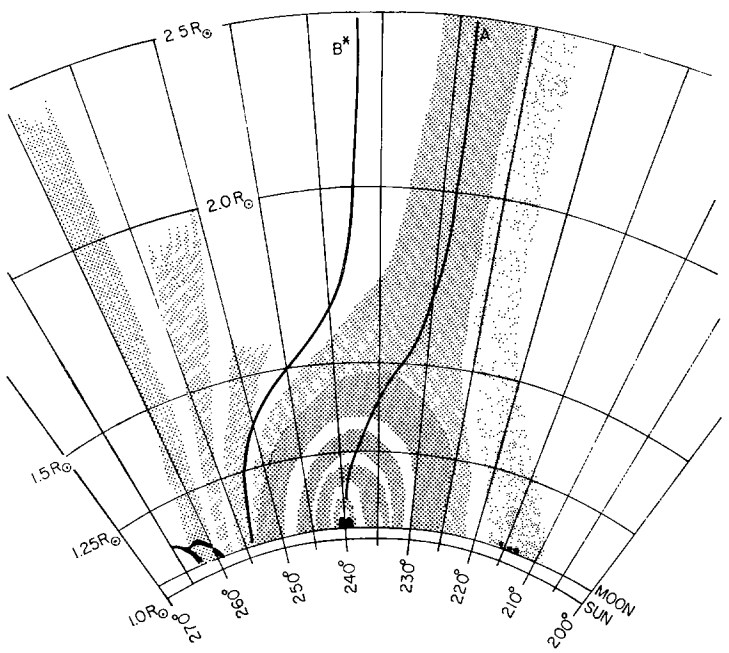


Fig. 3. A sketch of the multiple-arch system with coordinate network and limbs of the sun and moon. The arches are designated from inside out $a$, $b$, $c$, and $d$, respectively.

The multiple-arch system is composed of four components; the innermost two are partly superposed. Let us designate them as $a$, $b$, $c$, and $d$ from the inside outward. Roughly speaking, the arches are elliptic in shape with the center of the ellipse at the top of the underlying prominence. The dimensions of the arches are as follows:

(1) Heights: Average heights of the tops of the arches above the sun's limb are 0.18 $R_\odot$ for arch $ab$ blended, 0.27 $R_\odot$ for arch $c$, and 0.42 $R_\odot$ for arch $d$. The heights of three arches seen on the Von Klüber drawing are measured to be 0.10 $R_\odot$, 0.16 $R_\odot$ and 0.27 $R_\odot$ above the moon's limb. (The sun's limb is estimated to be 0.01 $R_\odot$ below

the moon's limb.) From the Balanovsky-Perepelkin sketch at the same eclipse, the innermost bright arch is estimated to be 0.10 $R_\odot$ above the moon's limb. Figure 9 in Kawaguchi's paper gives 0.09 $R_\odot$ above the moon's limb for the innermost border of a bright arch. He reports that the outer border of the arch is not clear. The height of the moon's limb above the sun's was about 0.01 $R_\odot$. Although there is a scarcity of available data, it is interesting to note that multiple arches are usually localized at 0.10 $R_\odot$, 0.18 $R_\odot$, 0.27 $R_\odot$ above the sun's limb. The height of arch $d$ is ambiguous because the value 0.42 $R_\odot$ obtained by visual estimation is quite different from photometric determination 0.36 $R_\odot$. A discussion of this problem will be given in Section 4. The discrepancy may come from a different visual weighting method in estimating the position of a faint object. The authors prefer 0.36 $R_\odot$ as the objectively determined value. So, the arches are distributed almost equidistant in height with an interval of 0.09 $R_\odot$.

(2) Widths: The widths of arches $a$, $b$ and $c$ are visually estimated to be about 0.03 $R_\odot$ at 0.10 $R_\odot$ above the sun's limb, while it is 0.07 $R_\odot$ for arch $d$ at the same height. At the tops the arches become asymmetric in brightness in the radial direction with lower brightness gradient outward and higher gradient inward from the central lines of the arches. The VON KLÜBER (1961) drawing gives 0.05 $R_\odot$ for the average width. Kawaguchi's value is also about 0.05 $R_\odot$. Figure 3 shows that the arches increase their widths with increasing heights. As will be described in Section 4, an objective evaluation of the width is possible; a parameter $\xi$ is defined as the distance along the concentric circle from the apparent center of arch where the brightness is maximum to the point where the brightness is $1/e$ of the maximum. In this case we deal with the brightness distribution of the arch proper $(B-B^*)$ after subtracting the background brightness $(B^*)$ from the observed value $B$ as shown in Figure 5 in Section 4. Taking the values of $\xi$ from Table II in Section 4 and multiplying them by $\cos i$, where $i$ is the inclination of the central line of the arch from the radial direction at respective heights, we obtain Figure 4. Figure 4 represents a variation of the half-width of respective arches $\xi' = \xi \cos i$ with height. The values at the tops of arches were computed from $\xi' = \xi \operatorname{cosec} i$ where $\xi$ and $i$ are obtainable from Table III in Section 4. Table III gives different values of $\xi$ inside and outside the central lines, so they are averaged. Figure 4 shows a tendency of broadening of the arches upward. They are on the average

$$\frac{\xi'_{\min}}{\xi'_{\max}} = \begin{cases} 0.40 \text{ for arch } ab \\ 0.42 \text{ for arch } c \\ 0.38 \text{ for arch } d. \end{cases}$$

These values are used in Section 7, where we interpret the arches as rod-shaped 'leaky magnetic bottles'.

(3) Flattenings: The flattening ($\varepsilon$) is defined as the ratio of the minor axis to the major axis of an arch. In the present case a point 0.03 $R_\odot$ above the sun's limb was assumed to be the common center of the arch ellipses. The position angle of this center is slightly different for different arches, but they are all very near P.A. 240° where the mother (daughter?) prominence exists. The height of 0.03 $R_\odot$ also corre-

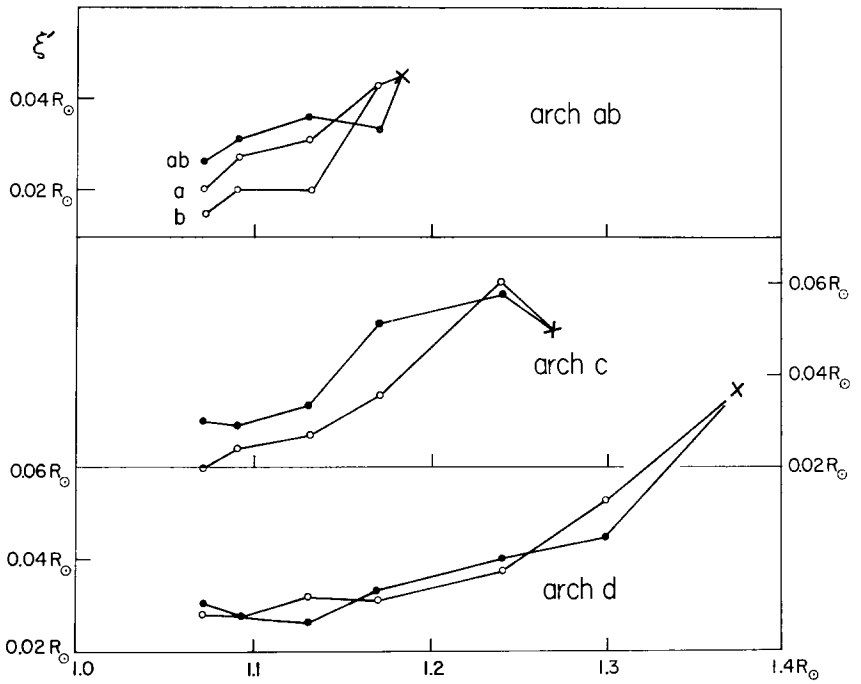


Fig. 4. Half-widths ($\xi'$) of respective arches. Broadening with height is evident. Black dots represent the values for the North branches, open circles for the South branches and crosses for the tops of arches.

sponds to the summit of this prominence. As the arches show only one-half of an ellipse above the sun's limb, it is hard to determine the flattenings accurately. Their tentative values are given in Table I. Measures obtained from drawings by other investigators are also given for comparison.

Let us compare the observed flattenings with those of the dipole magnetic-field lines from an idealized bar magnet whose length is $2l$. The lines of force are given by the following differential equation:

$$\frac{\mathrm{d}r}{r\,\mathrm{d}\phi} = \cot\psi = \frac{b^3 - a^3}{b^3 + a^3}\left(\frac{r}{l}\right)\operatorname{cosec}\phi - \cot\phi\,, \tag{1}$$

where $a^2 = r^2 + l^2 - 2rl\cos\phi$, and $b^2 = r^2 + l^2 + 2rl\cos\phi$. $r$ represents a radius vector from the bar center, $\phi$ an angle between the bar axis and radius vector, and $\psi$ an angle between the radius vector and the tangent at the line-of-force curve. If we choose the lines that are normal to the solar surface, i.e., $\psi = 90°$ at $r = l$ and $\phi = 0°$, we get a flattening of 0.577. This result is independent of the length of the bar. If we take the curvature of the surface of the sun into account, we expect that the outer arches may have a little less flattening than the computed value, even if they are initially normal to the limb. The value 0.38 in brackets in Table I is omitted because of its blending effect of arch *a* and *b*. The 1961 eclipse flattening value is similar to the 1962 values, while the 1927 eclipse values are 15% larger. We may conclude that

TABLE I

Observed flattenings ($\varepsilon$) of arches

| | | | | |
|---|---|---|---|---|
| 1962 eclipse (present data) | | | | |
| Average height | | 0.18 $R_\odot$ | 0.27 $R_\odot$ | 0.42 $R_\odot$ |
| $\varepsilon$ inner border | | (0.38) | 0.54 | 0.52 |
| $\varepsilon$ outer border | | 0.58 | 0.54 | 0.54 |
| 1927 eclipse (Von Klüber) | | | | |
| Average height | 0.10 $R_\odot$ | 0.16 $R_\odot$ | 0.27 $R_\odot$ | |
| $\varepsilon$ inner border | | 0.64 | 0.65 | |
| $\varepsilon$ outer border | 0.60 | 0.65 | 0.68 | |
| 1927 eclipse (Balanovsky-Perepelkin) | | | | |
| Average height | 0.10 $R_\odot$ | | | |
| $\varepsilon$ central line | 0.66 | | | |
| 1961 eclipse (Kawaguchi) | | | | |
| Average height | | 0.18 $R_\odot$ | | |
| $\varepsilon$ central line | | 0.56 | | |

the 1961 and 1962 eclipse arches may have been due to electron concentrations along field line arches seen almost normal to the line of sight, while the plane of the 1927 eclipse arches may have deviated from the celestial plane by 25° or so.

The multiple arches are concentric in shape. This differs from the behavior of loop prominences which are sometimes projected in all directions. VON KLÜBER (1932) sketched another multiple-arch system at P.A. 330° on the January 14, 1926 eclipse plate which is a little different from the above data. His system was composed of two concentric bright arches, almost egg-like in shape, with the tapered (narrow) end downward. The flattening values derived from his drawing are respectively 0.67 and 0.71 at the heights 0.13 $R_\odot$ and 0.29 $R_\odot$ above the top of included prominence. The heights of the tops of the arches above the sun's surface are unknown.

(4) Inclinations of axes: The semi-major axes of the present arches are a little inclined toward the South pole from normal. The inclination is 10° for arch *ab*, 14° for arch *c*, and 21° for arch *d*. The axes for the 1927 arches (Von Klüber, Balanovsky-Perepelkin) were inclined 8–10° toward the equator while for the 1961 arch (Kawaguchi) the angle of inclination was 9° toward the South pole. The arches at the 1926 eclipse (von Klüber) show no appreciable inclination of their axes.

(5) Separations along the limb: Average distances between the roots of arches are 0.035 $R_\odot$ or 24500 km on the sun's surface. This value is close to the average diameter of supergranules, i.e., 30000 km.

## 4. Photometric Results

By subtracting the brightness of background $B^*$ from the observed brightness $B$ in Figure 2 we obtain the heavy lines shown in Figure 5. We indicate the pattern of

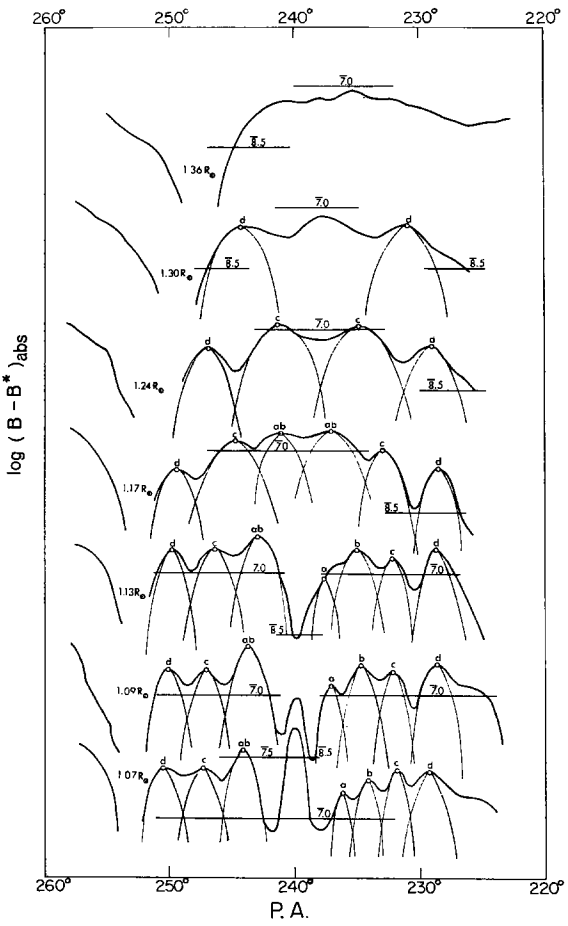


Fig. 5. Brightness distributions of the multiple-arch system ($B$ — $B^*$) along the helio-concentric arcs. Thin parabolic curves express Equation (2).

$\log(B-B^*)_{abs}$ in the logarithm at the following solar distances from bottom upward: 1.07 $R_\odot$, 1.09 $R_\odot$, 1.13 $R_\odot$, 1.17 $R_\odot$, 1.24 $R_\odot$, 1.30 $R_\odot$ and 1.36 $R_\odot$. Other curves in Figure 2 were used for reference to get the seven standard curves shown in Figure 5. The multiple arches are evident as the brightness maxima with designations of *a*, *b*, *c*, and *d*. The two maxima at P.A. 240° on the lowermost two curves at $r=1.07\ R_\odot$ and 1.09 $R_\odot$ come from a bright halo-finger, or halo-ridge, lying above the prominence.

Let us suppose these curves to be a composite of arches each with its brightness distributed along the arc concentric to the sun according to the Gaussian formula

$$B - B^* = E\, e^{-(x^2/\xi^2)}. \tag{2}$$

$x$ is the linear distance measured North or South from the maximum point along the concentric arc in units of $R_\odot$. $E$ is the maximum brightness on respective curves and $\xi$ is the parameter of width described earlier. When we take the logarithm, the right-hand

term in Equation (2) reduces to a parabolic form. The arches are superposed on each other's wings, so the fit of the curves to Equation (2) was made keeping in mind that the intersection of neighboring parabolas should be 0.30 below the observed curves in the logarithm. Final fits are the thin parabolic curves shown in Figure 5. The adopted values of $\log E$ and $\xi$ are given in Table II together with the position angles and inclinations. The fit for the 1.36 $R_\odot$ curve is absent because the trace is nearly tangent to the boundary of arch *d*.

The brightness distributions in the radial direction were also obtained along the axis of the arch system *A* and along the *B** valley shown in Figure 3. The photometric curves are shown in Figure 6 together with the $\log(B-B^*)$ curve. Note that the abscissae are not curvilinear lengths along the axis but radial distances from the sun's center. Fit with Equation (2) was tried along the radial direction. It turns out, how-

TABLE II

Position angles (P.A.), half-width ($\xi$), the maximum brightness ($E$) and inclination ($i$) of respective arches (horizontal cut)

| | North branch | | | South branch | | | |
|---|---|---|---|---|---|---|---|
| | *d* | *c* | *ab* | *a* | *b* | *c* | *d* |
| $r=1.07\ R_\odot$ | | | | | | | |
| P.A. | 250°.4 | 247°.2 | 244°.0 | 236°.1 | 234°.1 | 231°.8 | 229°.2 |
| $\xi$ | 0.030 | 0.031 | 0.027 | 0.015 | 0.020 | 0.020 | 0.030 |
| $\log E$ | $\bar{7}.40$ | $\bar{7}.40$ | $\bar{7}.55$ | $\bar{7}.20$ | $\bar{7}.31$ | $\bar{7}.41$ | $\bar{7}.38$ |
| $i$ | 17° | 10° | 9° | 2° | 2° | −5° | −6° |
| $r=1.09\ R_\odot$ | | | | | | | |
| P.A. | 250°.0 | 247°.0 | 243°.6 | 237°.0 | 234°.6 | 232°.1 | 228°.5 |
| $\xi$ | 0.030 | 0.030 | 0.032 | 0.020 | 0.028 | 0.024 | 0.028 |
| $\log E$ | $\bar{7}.20$ | $\bar{7}.21$ | $\bar{7}.40$ | $\bar{7}.08$ | $\bar{7}.25$ | $\bar{7}.20$ | $\bar{7}.26$ |
| $i$ | 18° | 13° | 13° | 5° | 7° | −3° | −4° |
| $r=1.13\ R_\odot$ | | | | | | | |
| P.A. | 249°.6 | 246°.3 | 242°.9 | 237°.5 | 235°.0 | 232°.1 | 228°.7 |
| $\xi$ | 0.029 | 0.036 | 0.038 | 0.021 | 0.034 | 0.027 | 0.032 |
| $\log E$ | $\bar{7}.19$ | $\bar{7}.20$ | $\bar{7}.30$ | $\bar{8}.98$ | $\bar{7}.20$ | $\bar{7}.13$ | $\bar{7}.20$ |
| $i$ | 22° | 20° | 22° | 13° | 18° | 7° | −2° |
| $r=1.17\ R_\odot$ | | | | | | | |
| P.A. | 249°.4 | 244°.8 | 241°.0 | 237°.0 | | 232°.9 | 228°.5 |
| $\xi$ | 0.036 | 0.038 | 0.042 | 0.054 | | 0.038 | 0.032 |
| $\log E$ | $\bar{8}.85$ | $\bar{7}.08$ | $\bar{7}.14$ | $\bar{7}.16$ | | $\bar{7}.00$ | $\bar{8}.86$ |
| $i$ | 25° | 25° | 40° | 35° | | 15° | 0° |
| $r=1.24\ R_\odot$ | | | | | | | |
| P.A. | 247°.0 | 241°.5 | | | | 234°.8 | 229°.0 |
| $\xi$ | 0.047 | 0.070 | | | | 0.070 | 0.050 |
| $\log E$ | $\bar{8}.84$ | $\bar{7}.03$ | | | | $\bar{7}.02$ | $\bar{8}.86$ |
| $i$ | 32° | 35° | | | | 30° | 13° |
| $r=1.30\ R_\odot$ | | | | | | | |
| P.A. | 244°.4 | | | | | | 231°.0 |
| $\xi$ | 0.062 | | | | | | 0.062 |
| $\log E$ | $\bar{8}.84$ | | | | | | $\bar{8}.86$ |
| $i$ | 43° | | | | | | 30° |

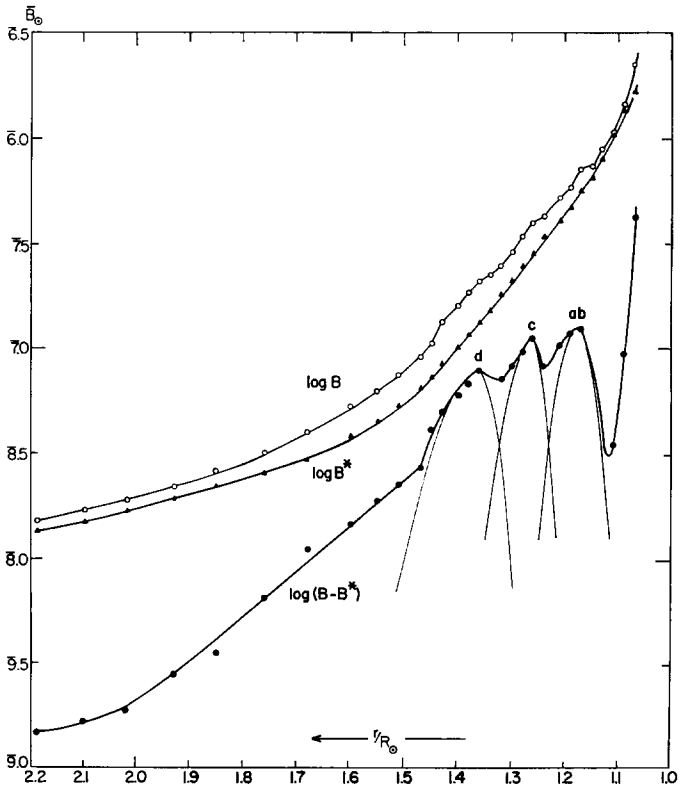


Fig. 6. Brightness distributions along the axis of the arch system $A$ and along the background $B^*$ with the resultant curve of log $(B - B^*)$. Radial sections of respective arches are indicated with $a$, $b$, $c$, and $d$. Note the coronal cavity at $r = 1.12\ R_\odot$.

ever, that as the curves are not symmetric with respect to the maximum points, respective arches should have different $\xi$ values inward and outward in order to get the best possible fit. The results are given in Table III.

The $\log(B - B^*)$ curve in Figure 6 shows a remarkable excess of brightness over the adopted Gaussian distribution outside 1.5 $R_\odot$ from the sun. This excess brightness

TABLE III

Position angles (P.A.), half-width ($\xi$), the maximum brightness ($E$) and inclination ($i$) along the axis of arch system $A$

| arch | *ab* | | *c* | | *d* | |
|---|---|---|---|---|---|---|
| | inside | outside | inside | outside | inside | outside |
| P.A. | 239° | | 237° | | 236° | |
| $\xi$ | 0.042 | 0.045 | 0.030 | 0.060 | 0.040 | 0.095 |
| $\log E$ | $\bar{7}.10$ | | $\bar{7}.05$ | | $\bar{8}.90$ | |
| $i$ | 70° | | 65° | | 60° | |

belongs to the halo enveloping the arch system and there is an outward extension like a streamer extending out into space.

Furthermore, there is a depression of $\log(B-B^*)$ at $r=1.12\ R_\odot$ to $1.13\ R_\odot$ above the prominence. Existence of this depression, or a dark coronal cavity, has been noticed by many observers. Though the space is about five times fainter when compared with the surrounding arches, it is 3% brighter than the background $B^*$ at equivalent heights.

## 5. Electron Density

Before proceeding to derive the electron densities in the arches, we must make up a three-dimensional model of the feature in question; whether it is a real arch, a tunnel, a dome, or any other form in order to characterize the line-of-sight extent of the arches. Although these features have been described as arches, they may have been dome- or tunnel-shaped. Von Klüber suggests that bright domes may be formed as a result of periodic ejections of electrons from the underlying prominence. In order to explain the flattening of the arches, the velocities would be larger in the radial direction and smaller in the horizontal directions. Kawaguchi, on the other hand, assumes they are doughnut-shaped, facing the line of sight and placed along a magnetic tube of force bridging the prominence. In addition, we assume that they are a multiple-tunnel system which envelops the underlying prominence. We discuss critically the observed aspects of each of these models and derive electron densities for possible arch models.

(1) Dome-like elliptical shells: Let us first suppose an idealized dome formation

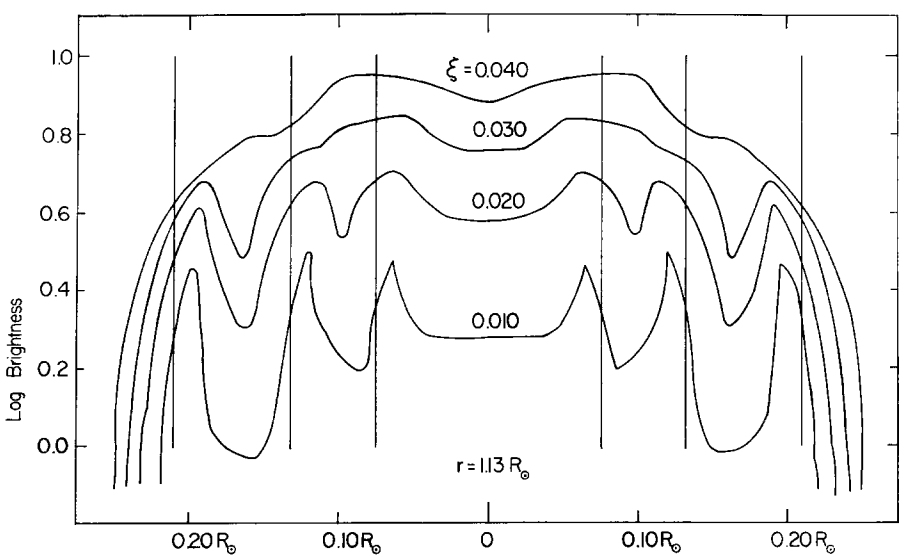


Fig. 7. Apparent brightness distributions of a triple bright dome viewed from a side. Half-widths of the dome walls are given as $0.010\ R_\odot$, $0.020\ R_\odot$, $0.030\ R_\odot$, and $0.040\ R_\odot$. The vertical lines indicate the wall centers.

which exhibits horizontal sections at $r = 1.13\ R_\odot$ that are composed of three concentric circular belts with a certain width. The radii of the belts are taken as $0.075\ R_\odot$, $0.133\ R_\odot$ and $0.209\ R_\odot$, respectively, to make them approach the observed values as closely as possible. Furthermore, if we suppose that these belts are uniformly populated with free electrons (non-uniform populations do not change our results significantly), we get Figure 7, which represents the apparent brightness distributions of the multiple-dome at the height of $r = 1.13\ R_\odot$. The four curves in the figure correspond, from the top down, to the cases where the half-widths of the shells equal $0.040\ R_\odot$, $0.030\ R_\odot$, $0.020\ R_\odot$ and $0.010\ R_\odot$, respectively. For simplicity the calculation was made graphically under the assumption that the apparent brightness is proportional to the sum of lengths in the line of sight which is included in respective belts.

The brightness distributions shown in Figure 7 show that the observed arch system could not be dome-shaped. The dome system would yield too large a contribution to the brightness of the apparent dome center, where the observed intensity is very low.

(2) Rod-like concentrations: Next, let us assume that the observed features are an aggregate of four concentric rods which are projected from the sun's edge with their central lines included in the celestial plane. Furthermore, let us assume that the rod is circular in horizontal section so that the light scattering electrons are distributed symmetrically to the center of rod:

$$N - N^* = N_0\, e^{-(\rho/\xi)^2}. \tag{3}$$

$N_0$ is the variable electron density at the center of rod; $N^*$ is the contribution from the K-corona and $\rho$ is the horizontal distance from the center of rod. The apparent brightness of the rod, viewed from the side, is

$$B - B^* = 2 \int_x^\infty \frac{N_0 C\, e^{-(\rho/\xi)^2}}{\sqrt{\rho^2 - x^2}}\, \rho\, \mathrm{d}\rho, \tag{4}$$

where

$$C = \tfrac{3}{8}\sigma \bar{B}_0 \left[A(1 + \cos^2\theta) + B \sin^2\theta\right]. \tag{5}$$

$A$ and $B$ in Equation (5) are the functions of solar distance and the limb-darkening coefficient, $q$. The numerical values are obtainable from Table III of the VAN DE HULST (1950) paper by taking $q = 0.75$. The cross-section of an electron ($\sigma$) equals $0.66 \times 10^{-24}$ cm$^2$. $\theta$ is an angle between the line of sight and the radius from the sun to the point in question. Since every possible value of $\theta$ lies between 88° and 92°, it is quite safe to take $C$ out of the integral sign in Equation (4).

Equation (4) is called Abel's integral and has a well-known solution:

$$B - B^* = C\sqrt{\pi}\, N_0 \xi\, R_\odot\, e^{-(x/\xi)^2}, \tag{6}$$

where axial symmetry has been assumed (see SAITO and BILLINGS, 1964). For $x = 0$,

$$E = C\sqrt{\pi}\, N_0 \xi\, R_\odot. \tag{7}$$

Data in Table II lead to the values of $N_0$.

If the distribution is elliptic in shape in horizontal section with $\xi$ and $\xi \cos i$ as

the semi-major axis in the celestial plane and the semi-minor axis in the line of sight, Equation (7) reduces to

$$E = C\sqrt{\pi} N_0 \xi R_\odot \cos i . \tag{8}$$

$\cos i$ should be replaced by $\operatorname{cosec} i$ in the case of radial section in Figure 6 or Table III. These modifications mean that the rod is a disk of radius $\xi \cos i$ normal to the central line. The results are given in Tables IV and V. Discrepancies between the values of $N_0$ in Table V inside and outside the central line of rod come from different $\xi$ values assigned to both sides.

TABLE IV

Log $N_0$ or electron density at the center of arch (rod model)

| $r/R_\odot$ | North branches | | | South branches | | | |
|---|---|---|---|---|---|---|---|
| | *d* | *c* | *ab* | *a* | *b* | *c* | *d* |
| 1.07 | 8.60 | 8.57 | 8.78 | 8.68 | 8.67 | 8.76 | 8.56 |
| 1.09 | 8.42 | 8.42 | 8.58 | 8.46 | 8.48 | 8.50 | 8.49 |
| 1.13 | 8.50 | 8.41 | 8.49 | 8.41 | 8.43 | 8.44 | 8.43 |
| 1.17 | 8.12 | 8.15 | 8.43 | 8.31 | | 8.23 | 8.14 |
| 1.24 | 8.11 | 8.14 | | | | 8.10 | 8.02 |
| 1.30 | 8.06 | | | | | | 8.00 |

TABLE V

Log $N_0$ at the tops of arches (rod model)

| | arch *ab* | | arch *c* | | arch *d* | |
|---|---|---|---|---|---|---|
| | inside | outside | inside | outside | inside | outside |
| mean $r/R_\odot$ | 1.16 | 1.20 | 1.24 | 1.29 | 1.33 | 1.42 |
| log $N_0$ | 8.18 | 8.24 | 8.40 | 8.14 | 8.12 | 7.88 |
| mean | 8.21 | | 8.27 | | 8.00 | |

Figure 8 shows the distribution of $\log N_0$ as a function of solar distance. Black circles represent the values for the North branches (i.e., larger values of P.A.), open circles those for the South branches, and crosses those for the tops of respective arches with both sides averaged. The central density sharply decreases according to the law $1/r^{12}$ around $r=1.1\ R_\odot$ but the rapid density gradient becomes diminished as we go outward, e.g., $1/r^{1.6}$ at $r=1.3\ R_\odot$. Empirical formulae applicable for $r$ between $1.05\ R_\odot$ and $1.40\ R_\odot$ are found to be:

$$\begin{aligned}
&\text{arch } ab: \quad N_0 = \frac{[9.35]}{r^{22}} + \frac{[8.35]}{r}, \\
&\text{arch } c: \quad N_0 = \frac{[9.26]}{r^{22}} + \frac{[8.26]}{r}, \\
&\text{arch } d: \quad N_0 = \frac{[9.20]}{r^{22}} + \frac{[8.20]}{r};
\end{aligned} \tag{9}$$

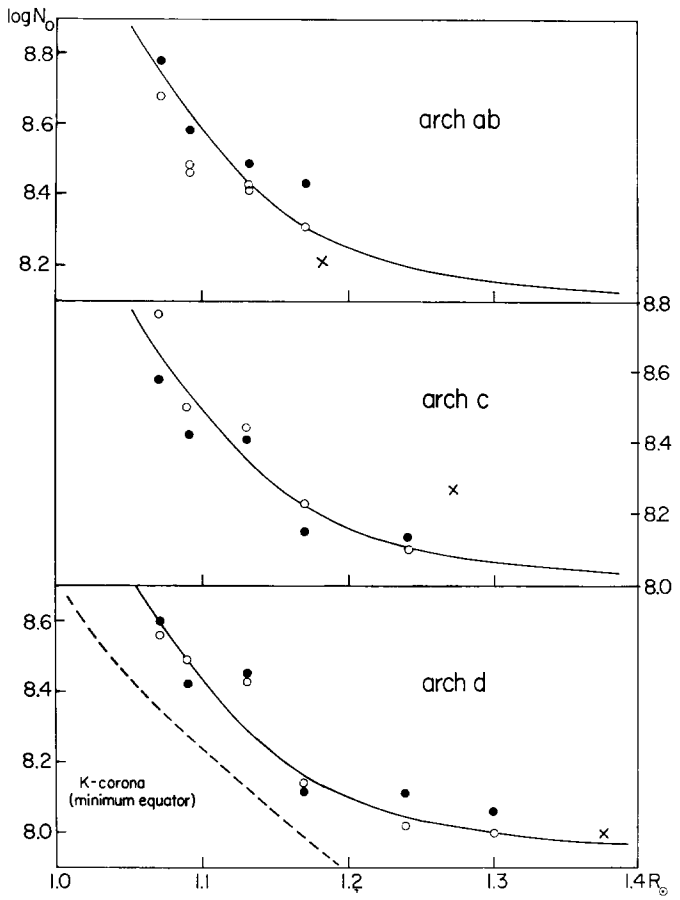


Fig. 8. Distribution of electron densities along the central lines ($N_0$) of respective arches in the case of the rod model.

where the square brackets mean the logarithmic numbers. It is interesting to note that all of the arches follow quite the same law of decrement but for different factors at $r=1.0\ R_\odot$. Electron densities along the North branches are not always equal to those in the South branches at the same heights, but they are averaged for simplicity. The solid curves in Figure 8 represent Equations (9), while the standard electron density in the K-corona (minimum and equator) is given in a broken line for comparison (NEWKIRK, 1967). From hydrostatic theory, we would conclude that the arches are at almost the same temperature as the K-corona for $r$ less than $1.2\ R_\odot$.

The total number of electrons ($\mathfrak{N}$) in a horizontal section 1 cm thick of respective arches is obtainable from

$$\mathfrak{N} = \pi(\xi R_\odot)^2 N_0 \cos i = \sqrt{\pi}\, \xi R_\odot \frac{E}{C}. \tag{10}$$

Figure 9 represents $\log \mathfrak{N}$ as a function of solar distance, again plotted with black

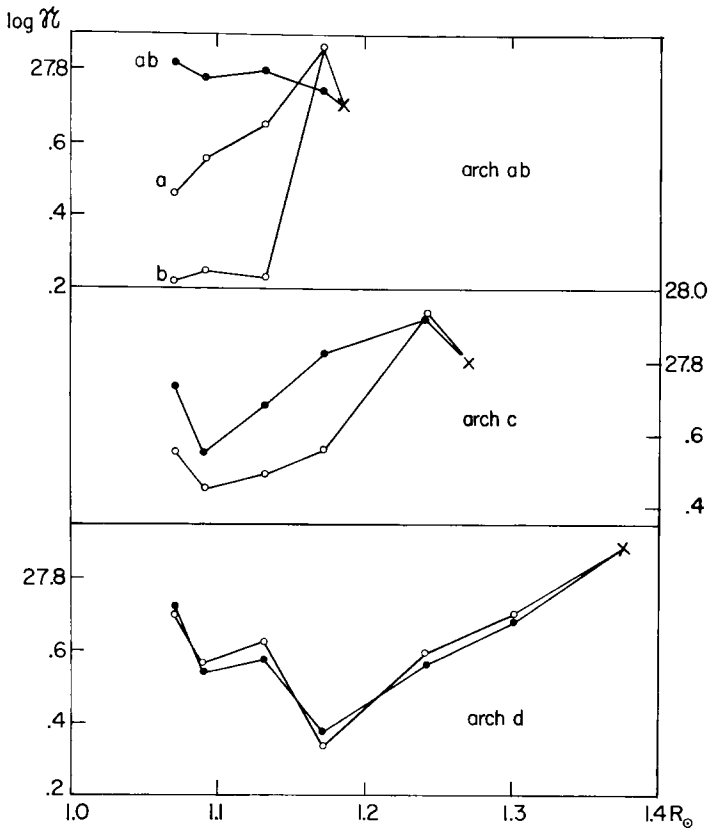


Fig. 9. Total number of electrons ($\mathfrak{N}$) included in a slice 1 cm thick for respective arches. The values of $\mathfrak{N}$ are independent of the model used.

circles for the North branches, open circles for the South branches and crosses for the tops of arches. Though some plots appear to show a certain tendency with solar distance, it would be dangerous to draw any conclusion unless accumulated possible errors were taken into account. It would be safer to mention that the average total number of electrons in a horizontal slice 1 cm thick of an arch is

$$3 \times 10^{27}/\text{cm}$$

throughout the lengths of arches with a factor of 2 uncertainty.

Integrating $\mathfrak{N}$ along the arch, the total number of electrons in each arch is calculated. The totals are

$$1.6 \times 10^{38} \text{ for arch } ab,$$
$$1.9 \times 10^{38} \text{ for arch } c,$$
$$2.3 \times 10^{38} \text{ for arch } d.$$

These values are used in Section 7, where trapping of the coronal electrons in the arches is considered.

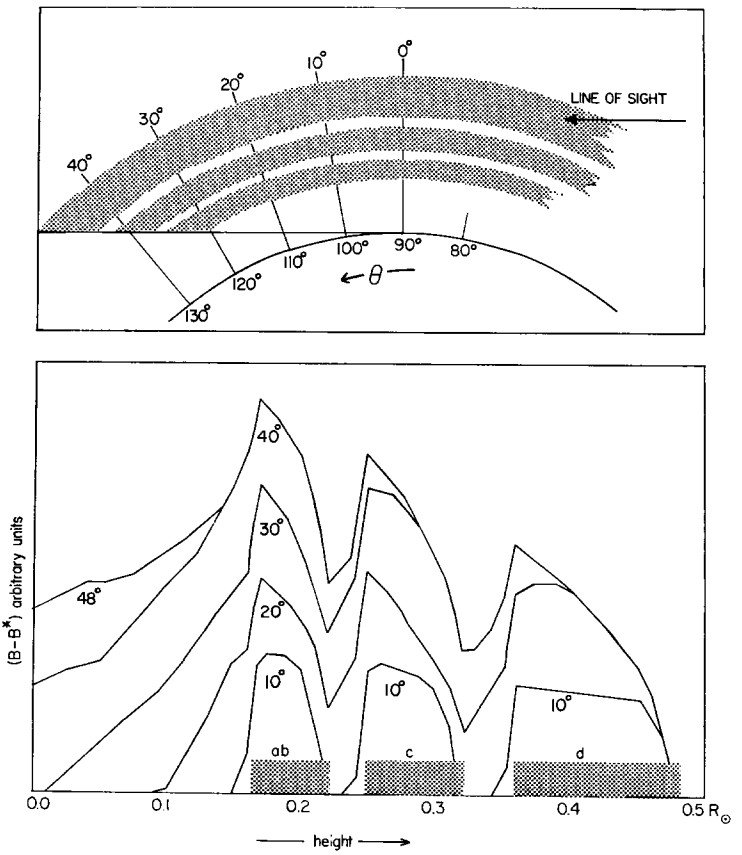


Fig. 10. Upper diagram: vertical section through a triple-tunnel system. Lower diagram: brightness in arbitrary units when viewed from the earth.

(3) Tunnel-shaped shells: We now check the possiblity that the observed arch system may be tunnel-shaped. If a multiple-tunnel system were seen head-on, it would have an appearance like the observed multiple-arch system. Let us take a simple model like that shown in the upper diagram of Figure 10. It represents a vertical section along the axis of a triple-tunnel system concentric with the sun's center. Respective tunnels have average heights and widths such as 0.19 $R_\odot$ and 0.05 $R_\odot$ for tunnel *ab*, 0.285 $R_\odot$ and 0.07 $R_\odot$ for tunnel *c*, and 0.42 $R_\odot$ and 0.12 $R_\odot$ for tunnel *d*. These numbers make the model fit the observations as well as possible. We suppose that the tunnels are uniformly filled with electrons at a certain density. Expected brightness distributions are shown in the lower diagram of Figure 10.

The formula necessary for evaluation is

$$B - B^* = \int_0^s NC(r, \theta)\, \mathrm{d}s, \tag{11}$$

where $s$ represents a tangential length in the line of sight counted from the vertical at $\theta=90°$. Evaluation of Equation (11) was carried out numerically, and the variability of $C$ was taken into account. In practice the tunnels were divided into several arcs, 10° long. A curve designated as 10° in the lower diagram gives the contribution from the tunnel of 10° interval from $\theta=90°$ to $\theta=100°$ or from $\theta=80°$ to $\theta=90°$. A curve designated as 20° is the equivalent quantity from a 20° interval from $\theta=90°$ to $\theta=110°$ or $\theta=70°$ to $\theta=90°$, and so on. For $\theta>120°$, the tunnel $ab$ becomes partly hidden by the sun's limb, and the whole system leaves the field of view around $\theta=138°$.

In case the tunnels are extended to both sides of the celestial plane, e.g., from $\theta=80°$ to $\theta=110°$, a simple addition of the contributions from the 10° and 20° intervals will give the correct result. We see from Figure 10 that the multiple tunnels are seen to be completely separated whenever $|\theta-90°|$ is less than 15°. When the tunnel is longer than this limit, an overlapping effect of curved tunnels comes into play. We have found in the previous section that the dark space at $r=1.13\ R_\odot$ above the prominence is $\frac{1}{5}$ as bright as the adjacent arches. The 20° curve in the diagram shows an excess brightness more than $\frac{1}{3}$ of that of the adjacent arches at $r=1.13\ R_\odot$, so the tunnels cannot be longer than $\pm 15°$ in arc from the celestial plane in the present case, but it is possible for the tunnel to exist between $80°\leq\theta\leq 110°$. In contrast with the dome model, Figure 10 shows that respective tunnels, arches, would appear well separated from each other.

According to the Hα filtergram data obtained during the two weeks prior to the eclipse day, a prominent dark filament was in the Southern hemisphere. It was a little curved and slightly inclined but laid almost parallel to the equator. This filament had been a majestic 700000 km long on January 29, 1962, but over the following days it fragmented and dissolved until the largest remnants visible on the disk near the West limb during February 3, 1962 were less than 50000 km long (i.e., much less than 15° extent along the line of sight). Also, the prominence that appeared on the East limb on January 20, 1962 was substantially larger and brighter than the prominence that appeared on February 4, 1962 at the focus of the arch system discussed here. Therefore, it seems reasonable to assume that the magnetic bridge system that may have accompanied the observed prominence did not have a line-of-sight extent greater than 15°.

Our model of the tunnel is that the solar surfaces on both sides of the dark filament have magnetically opposite polarities and that the tunnel-shaped formation is a set of magnetic bridges crossing over the filament. The coronal cavity exists where the field lines dip down into the prominence (see KIPPENHAHN and SCHLÜTER, 1957) and few, if any, electrons arrive in or remain in the cavity (they become trapped in the prominence). From the above-noted limitation on the length of the tunnel, the tunnel system now in question is supposed to extend along an interval from $\theta=90°$ to $\theta\leq 105°$ parallel to the equator. If we can ignore, for simplicity, the curvature of tunnels along the solar surface, and if we assume that the tunnel walls are filled with electrons (not uniformly but according to the Gaussian distribution to both sides from the middle of the breadth of wall), the following formula is valid:

$$B - B^* = N_0 \, e^{-(x/\xi)^2} \, Cs \,. \tag{12}$$

Figure 11 gives the values of $N_0$ for the tunnel model, which should be compared with $N_0$ for the rod model shown in Figure 8. In the range $r < 1.18\ R_\odot$, both models yield similar results, but the rod model gives an electron density that is five times larger than that of the tunnel model. For $r > 1.18\ R_\odot$, $N_0$ appears to be nearly constant with solar distance. The observed arches are thus explainable either as rods or tunnels that have line-of-sight dimensions less than 180000 km. The electron density at a given point is uncertain by a factor 5 between these two extreme cases. Therefore, our values bracket the minimum-equator densities given by Newkirk.

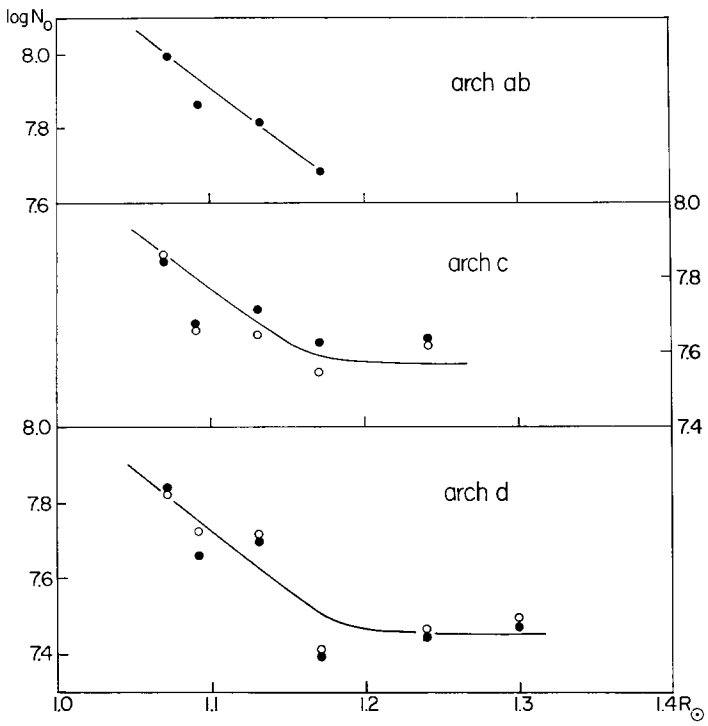


Fig. 11. Distribution of the central electron density ($N_0$) of respective arches in the case of tunnel model.

The total number of electrons ($\mathfrak{N}$) included in a horizontal slice 1 cm thick of one side of each tunnel is independent of model.

The arguments above lead us to the conclusion that the distinction between prominences that exhibit clearly defined arch systems and coronal cavities (e.g., the system discussed here) and those that do not (see Leroy and Servajean) could be geometrical. The prominences with *short* line-of-sight dimensions ($\Delta\theta < 20°$ or $l \leq 200000$ km) and small inclinations of the prominence axes with the line of sight would exhibit clearly defined arches and cavities. On the other hand, prominences

with *long* line-of-sight dimensions ($\Delta\theta > 20°$, or $l \geq 240000$ km) would exhibit much less pronounced cavities, regardless of the orientations of the prominence axes. If the axis of a *long* prominence were near the line of sight, however, it might be possible to see an arch system, but it would be somewhat confused, and there would not be a conspicuous coronal cavity immediately above the prominence. If the axis of the prominence made a large angle with the line of sight ($>25°$ for the short prominences and $>13°$ for the long prominences), both the distinct concentric arch system and the coronal cavity would become washed out due to superposition of projected structures.

## 6. Dark Cavity

Figure 5 shows that the dark coronal cavity above the prominence is darker than the surrounding arches by about 0.6 in the logarithm at $r = 1.13\ R_\odot$, but it still has a proper brightness of $\bar{8}.47\ \bar{B}_\odot$ in the logarithm.

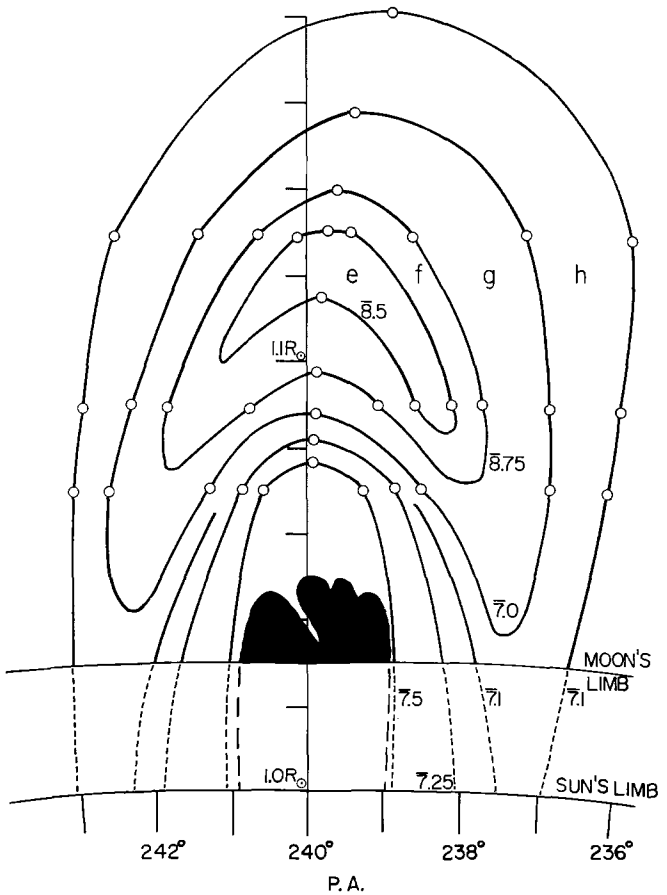


Fig. 12. Isophotic contour map of the coronal cavity above the prominence.

We examined several models and found that the cavity had a density that was about 18% of the central density of arch *ab*. This result seems to be roughly independent of the choice of model.

Now, we calculate in detail the total deficiency of electrons in the cavity. Figure 12 represents the isophotic diagram around the cavity. Data are obtained from Figures 5 and 6. Numbers assigned to the curves are the brightness values in units of $\bar{B}_\odot$. In Figure 6 we consider two curves: one curve touching the peaks of arches and the other touching the valleys. The values of the curves extrapolated to $r=1.13\ R_\odot$ are $\bar{7}.12\ \bar{B}_\odot$ and $\bar{8}.91\ \bar{B}_\odot$, respectively. These values are adopted as the upper and lower limits of the brightness level surrounding the cavity $(B-B^*)_{\text{surrounding}}$ from which the brightness depression of the cavity $(B-B^*)_{\text{cavity}}$ is measured. The isophotes $(B-B^*)_{\text{cavity}}$ are plotted in Figure 12.

We get the total deficiency of electrons in the cavity ($D$) from the formula

$$D=\sum_i \frac{S_i}{C}\left[(B-B^*)_{\text{surrounding}}-(B-B^*)_{\text{cavity}}\right]_i, \tag{13}$$

where $S_i$'s are the contour areas ($e, f, g$, and $h$) measured in units of cm$^2$ in Figure 12 and $C=1.51\times10^{-25}$ at $r=1.12\ R_\odot$. The number of electrons missing from the coronal cavity is found to lie between $1.5\times10^{37}$ and $0.38\times10^{37}$. It is noted here that the above results are independent of choice of the models and that $B^*_{\text{surrounding}}$ equals $B^*_{\text{cavity}}$ in Equation (13).

We have determined the number of electrons in the prominence, i.e., the excess ($E$) over the background corona, from slitless spectra taken near the third contact by the joint High Altitude Observatory, National Bureau of Standards and Sacramento Peak Observatory expedition to New Guinea during the February 4, 1962 eclipse (these plates are stored at Sacramento Peak Observatory). We used the spectra to avoid the contributions due to emission lines and to avoid the photographic saturation effects that plague pictures of prominences taken during eclipses (see Figure 1). We find that no continuum emission from the prominence could be detected on the slitness eclipse spectra. Thus we could not establish the excess of electrons in the prominence, but we did find the somewhat useless upper limit of $5\times10^{39}$ electrons in the prominence. This number is mentioned only because it is the only datum for the prominence that is based on specific observations.

We can do some calculations based on general properties of prominences, however, and arrive at order of magnitude values for the total number of electrons in the observed prominence. We consider two extremes: (1) The average electron density throughout the prominence is $1\text{–}3\times10^{10}$ cm$^{-3}$, and (2) the maximum electron density in the prominence $\{n_0$ in the equation $n_e=n_0\exp[-(h/H)]\}$ is $1\text{–}3\times10^{10}$ cm$^{-3}$, where the scale height ($H$) is between 3000 and 5000 km. For case (1) we find the excess ($E$) in the number of electrons in the prominence $0.5\leq E\leq1.5\times10^{38}$; for case (2) we find $1.3\leq E\leq4\times10^{37}$. Thus, we expect the excess number of electrons in the prominence to lie in the range $1.3\leq E\leq15\times10^{37}$. From this crude comparison we

find the ratio of the excess ($E$) to the deficiency ($D$) to be in the range

$$0.9 \leq \frac{E}{D} \leq 40. \tag{14}$$

Our study of the $E/D$ ratio, more than anything else, points to the need for coordinated eclipse studies of white-light photographic and polarimetric studies and spectrographic studies of prominence-(cavity?)-arch-streamer systems. With these data, we could determine values of $E/D$ for many different types and geometries of prominences at the limb, and perhaps obtain data that could lead to detailed theoretical models for prominences and their coronal environments.

## 7. The Problem of Trapping

We now speculate on the problem of the trapping of coronal ions in the arches (leaky magnetic bottle). If we assume that the arches are magnetic rods of radius $\xi'$ and that the arch structures correspond to magnetic-field lines, conservation of magnetic flux leads to

$$B_0(\xi'_0)^2 = B_h(\xi'_h)^2, \tag{15}$$

where $B_0$ and $B_h$ represent the magnetic-field strengths at the heights 0 and $h$ above the sun's surface, and $\xi'_0$ and $\xi'_h$ are the half-widths of the arches at the respective heights. Using the data given in Section 3, we find

$$\sin^2 \theta_c = \frac{B_{\min}}{B_{\max}} = \left(\frac{\xi'_{\min}}{\xi'_{\max}}\right)^2 = 0.16. \tag{16}$$

Therefore, $\theta_c = 24°$. $\theta_c$ is the critical pitch angle for trapping and $B_{\max}$ and $B_{\min}$ are the field strengths at the feet and tops of arches, respectively.

We find that the fraction ($\alpha$) of ions that escape the bottle is

$$\alpha = \int_0^{\theta_c} \sin\theta \, d\theta = 0.09. \tag{17}$$

If we let there be $n$ ions of a certain species (electrons or protons) and assume no charge separation to the first order, we can calculate the fraction of ions reflected, $\rho$, and the fraction transmitted, $\chi$, at the feet of the arches. The conditions

$$1 = \rho + \chi \quad \text{and} \quad \rho \gg \chi \tag{18}$$

exist. There are two characteristic times of importance: the average time ($\tau$) it takes for one of our specimens to cross from one foot of the arch to the other, and the characteristic time ($T$) over which the anisotropy that the leaky bottle tends to establish is made isotropic via collisions or some isotropic injection mechanism. For the time being we assume that only collisions are significant in redistributing the velocities of the ions. We consider the injection processes later in this section.

There are three broad cases to be considered (after THOMAS, 1958): (1) no collisions, $T \gg \tau$; (2) the intermediate case, $T \simeq \tau$; and (3) collisional domination, $\tau \gg T$. We consider rod-like shapes for the arches *ab*, *c* and *d* shown in Figure 3; we find $\bar{n}_e \simeq 2$ to $4 \times 10^8$ cm$^{-3}$. If we assume $T_e \simeq 10^6$ °K in the arches, we find $78 \leq \tau_e \leq 171$ secs and $2 \times 10^4 \leq \tau_p \leq 4 \times 10^4$ secs are the times required for electrons ($\tau_e$) and protons ($\tau_p$) to move from one foot to the other in the arches. We also find that the mean time between collisions in the arches is about 1 sec. Therefore, we find $\tau \gg T$ in all cases and for our purposes the system is collisionally dominated. Thus, an isothermal corona can explain the observed similarity in coronal scale heights in and out of the arches. The general solutions for $\rho$ and $\chi$ are

$$\rho = (1 - \alpha)\, e^{-(\gamma\Gamma\alpha/\gamma + \Gamma)t}, \tag{19}$$

$$\chi = \frac{\alpha}{\gamma + \Gamma}\, \Gamma\, e^{-(\gamma\Gamma\alpha/\gamma + \Gamma)t} + \gamma\, e^{-(\gamma + \Gamma)t}, \tag{20}$$

where $\gamma = 1/\tau$, $\Gamma = 1/T$ and $t \gg 0$, i.e., far removed from the initial conditions.

In the case of collisional domination, $\gamma \ll \Gamma$, Equations (19) and (20) for $\rho$ and $\chi$ become

$$\rho \cong (1 - \alpha)\, e^{-\gamma\alpha t} \tag{21}$$

and

$$\chi \cong \alpha\, e^{-\gamma\alpha t}. \tag{22}$$

Since $\rho + \chi = 1$, the time variation of the number of ions ($n_a$) in a rod-shaped arch due to losses of ions at the feet of the arches is

$$n_a = n_0\, e^{-\gamma\alpha t} \tag{23}$$

in the absence of any supply of ions into the arches. Therefore, if the number of ions within an arch is to remain constant, there must be a supply of ions ($n_g$) such that the demand equals the supply:

$$n_0 \chi|_{t=0+} = n_g, \quad \text{or} \quad n_g = n_0 \alpha, \tag{24}$$

(see Equation (22)), and $n_0$ is not a function of time. The time over which $n_g/e$ ions must be supplied to each arch is $1/\alpha\gamma$, or $\tau/\alpha$ sec. As shown above, $\tau \simeq 100$ sec; therefore, the relaxation time for these coronal arches is $\simeq 100/\alpha$, or about $10^3$ secs, and the net influx must be $5 \times \simeq 10^{34}$ electrons/sec. The mean area of the feet of the arches is $\pi\xi^2$ which is about $1.54 \times 10^{18}$ cm$^2$ or about a factor of 1 larger than the area covered by DUNN's (1960) *spicule porcupines* (*rosettes*; see BECKERS, 1964) at the junction of three or more supergranule cell boundaries.

Since the areas of the feet of the arches compare favorably with Beckers' *spicule rosette* areas and the mean separation between adjacent feet is somewhat less than the average supergranule diameter (see LEIGHTON *et al.*, 1962), we test the possible influx of matter into coronal arches from *spicule bushes* (see CRAGG *et al.*, 1963) situated at the feet of the arches. We assume individual spicules with outward velocities of 20 km/sec, electron densities of $10^{11}$ cm$^{-3}$ and cross-sectional areas of

$7.0 \times 10^{15}$ cm$^2$ ($7.0 \times 10^5$ km$^2$). Beckers counts an observed average of 15 spicules per *rosette*, but he states that due to observational selection this number is a factor of 4 too low. We assume, therefore, that the number of spicules feeding each arch is 120; 60 in each of 2 *rosettes*, one feeding each foot of an arch. These values lead to an upper limit for $n_g = \text{const} \simeq 2 \times 10^{35}$ electrons/sec that rise into the corona through the feet of an arch via spicules. This influx number of electrons is a factor of 4 higher than the above coronal arch efflux value.

Since most spicules are thought to return to the chromosphere, the total influx of electrons into a coronal arch from two *rosettes* should be significantly less than the value calculated above. On the other hand, the electrons in the observed arch may be displaced along the line of sight as in the tunnel model. In that case, we should diminish the efflux from a rod-shaped arch in the corona by some unknown factor, but then we should have to explain why all of the arches along the line of sight appear to line up and appear as one, etc.

Since there is near agreement between spicule influxes and arch effluxes at the feet of the arches, the supergranule diameters match the separations between adjacent arches, the dimensions of the arches near the chromosphere match the dimensions of *spicule porcupines*, *rosettes* and *spicule bushes*, the intensity decrements are the same in the arches, and the total number of electrons in each arch is about the same; it appears probable that the observed arches are rod-like in form and that we can expect the observed coronal rods to be visible manifestations of magnetic rods that exist between *spicule bushes* located approximately symmetrically on opposite sides of a prominence. In view of these arguments we expect the electron density distribution in the observed coronal arches to mimic closely the curves shown in Figure 8.

The close agreement between the spicule influx values and the collisionally dominated arch efflux values lea dsus to the conclusion that spicules are indeed the sources of electrons, and therefore protons, etc., in the corona, and that the densities in the coronal arches adjust themselves until equilibrium between the spicular influx and arch efflux is achieved.

The analysis outlined above needs testing, but again detailed and precision photographic, spectrographic and polarimetric data are needed to resolve completely the problems that we have blithely assumed away.

We conclude from all of the above analyses that the rod-like model for coronal arches is the best model of the three examined, but the tunnel model is not definitely excluded. It is possible, however, that spicules are not the source of the electrons observed in coronal arches; therefore, our analyses would not yield a clear distinction between the tunnel and the rod models for the observed arches. The dome-like model is excluded in any case where a coronal cavity is observed or when adjacent coronal arches are distinctly separated in intensity.

We suggest that the 1000 sec relaxation time for coronal arch densities to change by a factor of $e$ may be observable during solar eclipses of long duration, e.g., in 1973 (7 min) and in 1976 (5 min). These durations can be extended indefinitely by observing from satellites (see Newkirk) or by a factor of 2 by observing from jet aircraft flying

along the eclipse path. It is unlikely, however, that the birth or death of an arch will be observed during the short observing periods provided by total eclipses of the sun. The long lifetimes ($\simeq$21 hours) of supergranules and their associated *spicule bushes*, or *rosettes*, indicate that the 1000 sec (15 min) growth and decay periods occupy only 1/50 of the lifetimes of arches; that is, provided arches are indeed fed by and in equilibrium with particle fluxes from spicules.

## Acknowledgements

The authors are grateful to Dr. N. Owaki, who placed the eclipse plate at the authors' disposal. They also owe thanks to Dr. Frank Orrall and Dr. William Henze who enabled them to use the eclipse spectrum calibrations in advance of publication. One of the authors (K. S.) expresses his thanks to Dr. J. W. Evans, who invited him to the Sacramento Peak Observatory to use the microphotometer.

## References

BALANOVSKY, J. and PEREPELKIN, E.: 1928, *Monthly Notices Roy. Astron. Soc.* **88,** 740.
BECKERS, J. M.: 1964, AFCRL Environmental Research Paper No. 49, Sacramento Peak Observatory.
CRAGG, T., HOWARD, R. and ZIRIN, H.: 1963, *Astrophys. J.* **138,** 303.
DUNN, R. B.: 1960, Dissertation, Harvard University (= Sacramento Peak Obs. Contr. No. 87, 1965).
KAWAGUCHI, I.: 1967, *Solar Phys.* **1,** 420.
KIPPENHAHN, R. and SCHLÜTER, A.: 1957, *Z. Astrophys.* **43,** 36.
LAFFINEUR, M., BLOCH, M. and BRETZ, M.: 1961, *Sky and Telescope* **21,** 195: also see D. E. Billings, *A Guide to the Solar Corona* (1966), Academic Press, New York, pp. 16 and 20.
LEIGHTON, R. B., NOYES, R. W. and SIMON, G. W.: 1962, *Astrophys. J.* **135,** 474.
LEROY, J. L.: 1966, *L'astronomie* **80,** 271.
LEROY, J. L. and SERVAJEAN, R.: 1966, *Ann. Astrophys.* **29,** 263.
MALVILLE, J. M.: 1967, *Sky and Telescope* **23,** 136.
NEWKIRK, G., Jr.: 1967, 'Structure of the Solar Corona', *Ann. Rev. Astron. Astrophys.* **5,** 213.
OWAKI, N. and SAITO, K.: 1967, *Publ. Astron. Soc. Japan* **19,** 279.
SAITO, K. and OWAKI, N.: 1967, *Publ. Astron. Soc. Japan* **19,** No. 4.
SAITO, K. and BILLINGS, D. E.: 1964, *Astrophys. J.* **140,** 760.
SAITO, K. and HATA, S.: 1964, *Publ. Astron. Soc. Japan* **16,** 240.
SMITH, S. *et al.*: 1965, *AAS-NASA Solar Eclipse Symposium*, NASA Ames Research Center, Moffett Field, California.
THOMAS, R.: 1958, unpublished lectures on 'Leaky Magnetic Bottles', University of New Mexico.
VAN DE HULST, H. C.: 1950, *Bull. Astron. Inst. Neth.* **11,** 135.
VON KLÜBER, H.: 1932, *Z. Astrophys.* **4,** 1.
VON KLÜBER, H.: 1961, *Monthly Notices Roy. Astron. Soc.* **123,** 61.